IEEE Access
Multidisciplinary | Rapid Review | Open Access Journal

SPECIAL SECTION ON INTELLIGENT SENSING ON MOBILE AND SOCIAL MEDIA ANALYTICS

Received January 3, 2017, accepted January 19, 2017, date of publication February 6, 2017, date of current version March 13, 2017.

Digital Object Identifier 10.1109/ACCESS.2017.2664103

A New Single Image Super-Resolution Method Based on the Infinite Mixture Model

PEITAO CHENG[1], YUANYING QIU[1], XIUMEI WANG[2], AND KE ZHAO[1]

[1]School of Mechano-Electronic Engineering, Xidian University, Xi'an 710126, China
[2]School of Electronic Engineering, Xidian University, Xi'an 710126, China

Corresponding author: X. Wang (wangxm@xidian.edu.cn)

This work was supported in part by the National Natural Science Foundation of China under Grant 61472304 and Grant 61571343 and in part by the Fundamental Research Funds for the Central Universities under Grant JB150407.

ABSTRACT As a powerful nonparametric Bayesian model, the infinite mixture model has been successfully used in machine learning and computer vision. The success of the infinite mixture model owes to the capability clustering and density estimation. In this paper, we propose a nonparametric Bayesian model for single-image super-resolution. Specifically, we combine the Dirichlet process and Gaussian process regression for estimating the distribution of the training patches and modeling the relationship between the low-resolution and high-resolution patches: 1) the proposed method groups the training patches by utilizing the clustering property of Dirichlet process; 2) the proposed method relates the low-resolution and high-resolution patches by predicting the property of Gaussian process; and 3) the mentioned two points are not independent but jointly learned. Hence, the proposed method can make full use of the nonparametric Bayesian model. First, the Dirichlet process mixture model is used to obtain more accurate clusters for training patches. Second, Gaussian process regression is established on each cluster, and this directly reduces the computational complexity. Finally, the two procedures are learned simultaneously to gain the suitable clusters with the ability of prediction. The parameters can be inferred simply via the Gibbs sampling technique. Thorough super-resolution experiments on various images demonstrate that the proposed method is superior to some state-of-the-art methods.

INDEX TERMS Super-resolution, Dirichlet process, Gaussian process regression, Gibbs sampling.

I. INTRODUCTION

SINGLE image super-resolution has been successfully used in various computer vision applications [1]–[3]. It is remained a fundamental task in computer vision for different image degradation causes, such as optical blurring, motion blurring, and noising. In general, super-resolution methods can be divided into three categories: interpolation-based, regularization-based and example-based methods [4], [5]. Interpolation-based methods recover the degradation image through some upscale algorithms based on smooth functions, such as piecewise smooth [6] and smooth kernel [7]. Regularization-based super-resolution methods pay more attention on sequence images. This kind of methods aim at deblurring by constructing the regularization based on local or nonlocal constrains [8]–[11]. Example-based methods establish the mapping function between the LR patches and HR patches through machine learning algorithms. Most of the learning-based super-resolution methods utilize the dictionary or example which draw more attention in recent research, especially for single image super-resolution [5], [12]–[15].

Example-based single image super-resolution methods provide good frameworks to represent the local structure of images by patches or features. The recent and popular example-based methods involve two kinds, neighbor embedding approaches [16]–[18] and sparse coding approaches [13], [19], [20]. Neighbor embedding approaches usually model the relationship between the LR and HR patches with subspaces learning or manifold methods. The LR patches are potentially considered as low-dimensional embedding of HR patches. The sparse coding approach is first introduced to super-resolution by Yang *et al.* [19]. With the help of sparse representation, sparse coding based SR approaches can learn compact LR and HR dictionaries via regularized optimization. In order to achieve high quality HR image with detail texture and structure information, example-based SR methods require large and abundant datasets to generate the adequate dictionaries. However, the large dataset will induce series problems in the process of super-resolution. Firstly, for a LR patch, the nearest neighbor search would need much computation time, and at the same time, the performance of search results may be influenced. Secondly, large

patch datasets will make the correspondence relationship between LR and HR patches ambiguity, such as different HR patches may generate same LR patch due to the reason of down sampling. Thirdly, exampled-SR methods usually train the mapping functions from the space of LR patches to the space of HR patches. Given the large training dataset, the selection of mapping function or machine learning model is very difficult.

In this paper, we propose a novel algorithm for example-based single image super-resolution based on the infinite mixture model. The proposed algorithm focuses on different type of way to model the training samples. Using the grouping performance of Dirichlet process, the large number of LR/HR training patches will be clustered as active nodes. Then for each cluster, we establish the relationship between LR patch and the pixel point in HR patch using Gaussian process regression. The Gaussian process regression can give more accurately mapping function from patch to center pixel in HR patch rather than from patch to patch. On the other hand, the computation complexity of mapping function is determined by the number of patches in each cluster, which would lower than that on the whole patches.

The rest of the paper is organized as follows. Several related works are given in Section II. Section III introduces the proposed super-resolution model and its parameter inference. Section IV presents the experimental results. Finally, the conclusions are reached in section V.

II. RELATED WORKS

In recent years, there have been extensive works on single image super-resolution in machine learning and computer vision. In general, existing methods can be classified into two main categories: parametric models and nonparametric models. We will review some related works in two kinds in the following.

A. PARAMETRIC MODELS

Parametric models target on designing a batch learning algorithm from LR patches/space to HR patches/space. The model parameters are determined in the training process and they are considered as fixed values. Most of example-based SR methods belong to parametric models, such as neighbor embedding approaches and sparse coding approaches.

B. NONPARAMETRIC MODELS

Unlike parametric models, nonparametric methods provide series of statistical methods, which estimate the parameters as random variables. Therefore, nonparametric models require no or very limited assumptions to be made about the data. By contrast with parametric models, nonparametric models have drawn more attentions in recent years.

Tipping and Bishop propose generative Bayesian SR model for multiframe images [21], which estimates the unknown point spread function with a Gaussian process prior over images. As well known, Gaussian process is widely used as nonparametric priors on functions in probabilistic models. Gaussian process regression (GPR) is one of the most popular examples in Bayesian nonparametric models for their powerful generalization capability and intuitive probability interpretation. In recent years, GPR has been introduced to the framework of image SR. He et al. use GPR for predicting each pixel in HR image by its neighbors [22]. The performance of the method is restricted because the high-resolution image is produced from a single low-resolution image without any external training set. Then some extend SR works are proposed for large scale external training sets and low computational complexity, such as semi-local Gaussian process [23], active-sampling GPR [24] and prototype-based GPR [25].

Dirichlet process (DP) is another prominent representative which is widely used in nonparametric models. Compared with GP, DP or DP mixture model (DPMM) is able to flexibly adapt to the data. Zhou et al. propose a nonparametric Bayesian dictionary learning method for dealing with incomplete and noisy images [26]. Akhtar et al. extend the dictionary learning to hyperspectral image super resolution [27].

While few attempts have been made towards nonparametric Bayesian super-resolution methods, there are some problems cannot be neglected. Firstly, due to the restriction of the inputting images without any external training set, the performance of super-resolution results would be influenced [22]. Furthermore, aim to obtaining the target HR image with rich texture and edge details, some dictionary learning based super-resolution methods have been proposed [28]–[30]. The LR/HR dictionaries are often learned from observed LR/HR pairs. Then it is very important to obtain a good representative dictionary. Most existing dictionary learning methods are based on the finite distributions, such as Gaussian distribution and Gaussian mixture distribution, and they deal with the observed patches as finite clusters. This would limit the ability of the dictionary to represent image details. Finally, the processes of training dictionary and correlating between LD/HR images are independent, so it may be difficult to preserve the consistency of two processes. In other words, the dictionary learning should be related to the latter SR process, which can improve the quality of SR images.

In this paper, we develop a nonparametric Bayesian single image super-resolution method. The model combines the clustering property of DPMM and the powerful predicting property of GP. The DP-GPR super-resolution method partitions the training dataset into several clusters and learns a regression procedure for each cluster. The clustering procedure and GPR are jointly learned to gain the clusters with the ability of prediction.

III. PROPOSED WORK

In this section, we present the details of the proposed DP-GPR method. For convenient expression, we first give the notations used in the following.

Let X_L and Y_H be the training LR patches and desired HR patches respectively, where $X_L = \{x_{L,i}\}_{i=1}^{N} \in R^{d\times N}$ and $Y_H = \{y_{H,i}\}_{i=1}^{N} \in R^{D\times N}$. The LR set $X_L = \{x_{L,i}\}_{i=1}^{N}$ is interpolated the same size with $Y_H = \{y_{H,i}\}_{i=1}^{N}$, i.e., $X_{LH} = \{x_i\}_{i=1}^{N} \in R^{D\times N}$. At the same time, draw the center pixel of each patch $y_{H,i}$ and denote as y_i. Initial training samples with $\{x_i, y_i\}_{i=1}^{N}$. The testing LR image Ican also be represented with patch set $\{I_i\}_{i=1}^{M}$.

A. DIRICHLET PROCESS

The DP is a simply extension of the Dirichlet distribution to continuous spaces, which has been widely used for density estimation and clustering [31], [32]. We will cluster the training LR dataset X_{LH} using DPMM in the proposed super-resolution model.

The DP is defined by two parameters, a positive concentrate scalar α and a probability base measure G_0. Assuming the observed sample Y draws from a DPMM, the distribution of the dataset with parameter θ_j can be defined through $G \sim DP(G_0, \alpha)$. The DP model can be expressed as follows,

$$\begin{aligned} x_j &\sim p\left(x_j \left|\theta_j\right.\right), \\ \theta_j &\sim G, \\ G &\sim DP(\alpha, G_0). \end{aligned} \tag{1}$$

Given the training dataset and the number of the clusters K, DP is adapted to present the mixture distribution. Without loss of generality, the prior of base measure is defined with normal Wishart distribution. By utilizing the stick-breaking construction, the DPMM can be expressed as

$$\begin{aligned} v_k \left|\alpha\right. &\sim Beta(1, \alpha), \\ \theta_k \left|G_0\right. &\sim G, \\ z_j \left|\theta(\pi)\right. &\sim \text{Multi}(\theta(\pi)),\ x_j \left|z_j = k\right. \\ \theta_k &\sim p(Y \left|\theta_k\right.). \end{aligned} \tag{2}$$

where $\pi_j = v_j \prod_{k=1}^{j-1}(1 - v_k)$ and z_j is an indicator variable. If $z_j = k$, the sample x_j belongs the cluster k. For the finite training dataset, the number of clusters is fixed, then discrete distribution $G = \sum_{k=1}^{\infty} \pi_k \delta(\theta, \theta_k)$.

B. GAUSSIAN PROCESS REGRESSION

In the proposed method, the training dataset will be first clustered by the DPMM. For each cluster, the distribution of samples is represented with Gaussian distribution. Then we will use GPR to establish the relationship between the LR and HR patches.

GPR has been proven to be a powerful method for supervised learning. It defines a smooth mapping $f$on function space by the mean function $m(x)$and covariance function $k\left(x_i, x_j\right)$,

$$f \left|X\right. \sim GP\left(m(x), k\left(x_{i,}, x_j\right)\right). \tag{3}$$

where $k\left(x_i, x_j\right)$ composes the covariance matrix $K(X, X)$ with $K_{i,j} = k\left(x_i, x_j\right)$. Given a GP prior on f and Gaussian noise ε on the observation y, the GPR model can be represented as

$$y = f(x) + \varepsilon, \varepsilon \sim N\left(0, \sigma_n^2\right) \tag{4}$$

For a testing x^*, the joint distribution of the training output Y and the testing output y^* can be written as

$$\begin{bmatrix} Y \\ y^* \end{bmatrix} \sim N\left(0, \begin{bmatrix} K(X,X) + \sigma_n^2 I & K(X, x^*) \\ K(x^*, X) & K(x^*, x^*) \end{bmatrix}\right). \tag{5}$$

Then the prediction formulation for y^* can be written as mean value and covariance,

$$y^* \left|X, Y, x^*\right. \sim N\left(\overline{y^*}, var(y^*)\right). \tag{6}$$

where $\overline{y^*} = K(x^*, X)\left[K(X, X) + \sigma_n^2 I\right]^{-1} y$, and $var(y^*) = K(x^*, x^*) - K(x^*, X)\left[K(X, X) + \sigma_n^2 I\right]^{-1} K(X, x^*)$. In the learning process, the similarity between the samples is measured by the kernel function,

$$K\left(x_i, x_j\right) = \sigma_f^2 \exp\left(-\frac{1}{2}\frac{\left(x_i - x_j\right)^T \left(x_i - x_j\right)}{\gamma^2}\right). \tag{7}$$

The hyperparameters $\lambda = \left\{\sigma_n^2, \gamma, \sigma_f^2\right\}$of the GPR can be induced by maximizing the posterior which is proportional to the marginal likelihood,

$$p(\lambda \left|X, Y\right.) \propto p(Y \left|X, \lambda\right.). \tag{8}$$

That is, $\lambda = \left\{\sigma_n^2, \gamma, \sigma_f^2\right\}$ can be chosen by optimizing the marginal log-likelihood,

$$\begin{aligned} \log p(Y \left|X, \lambda\right.) = &-\frac{1}{2}\log\left|K(X,X) + \sigma_n^2 I\right| \\ &-\frac{1}{2}Y^T\left(K(X,X) + \sigma_n^2 I\right)Y - \frac{n}{2}\log 2\pi. \end{aligned} \tag{9}$$

The main limitation of GPR is the computational complexity, and the reason is that reference requires inversion of the matrix in equation (6). Given a $n \times n$ matrix, the time complexity of inversing the matrix is about $O\left(n^3\right)$.

C. THE DP-GPR SUPER-RESOLUTION MODEL

In this subsection, we will represent the proposed DP-GPR super-resolution method in detail. As shown in the above subsection, the computational complexity of GPR is determined by the number of training samples. So if the training dataset is divided into some clusters, the number of samples in each cluster is much smaller than that in the whole dataset. Therefore, if the GPR is implemented on clusters, the computational complexity would be significantly reduced.

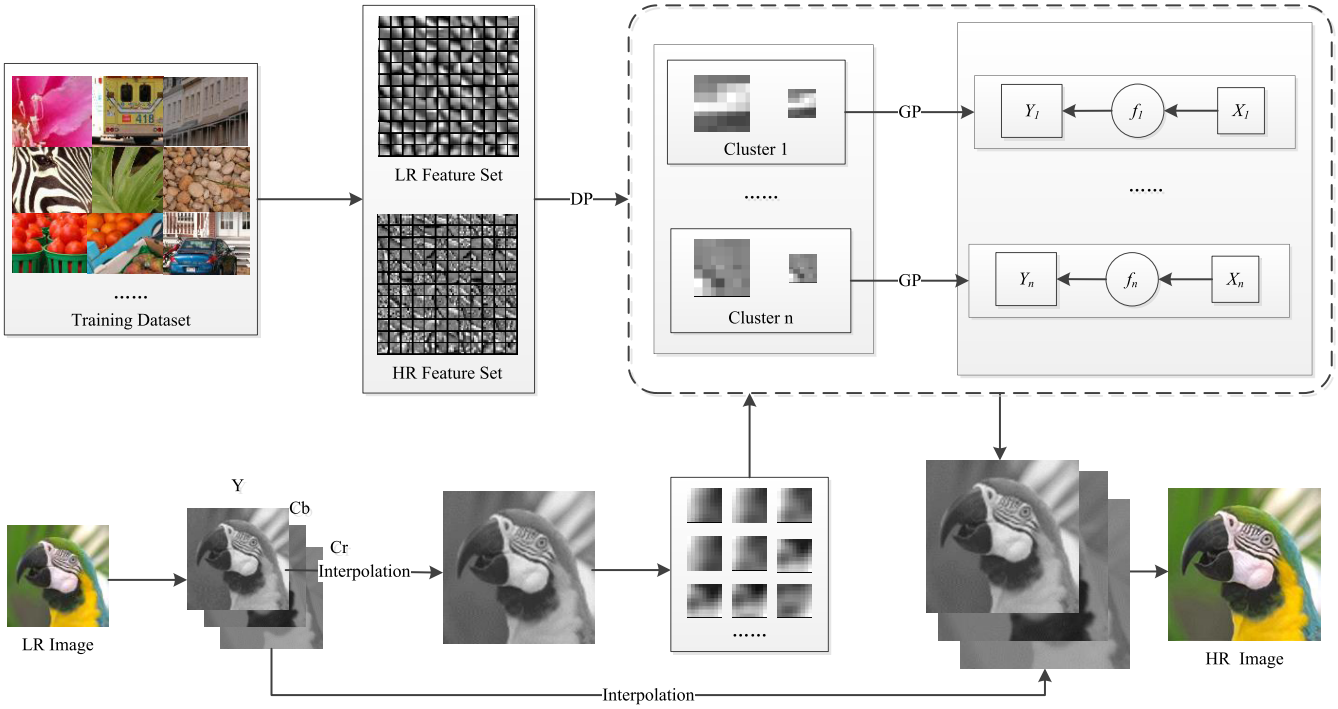

FIGURE 1. **The flowchart of the proposed method.**

According to the DPMM in equation (2) and GPR in equation (4), DP-GPR super-resolution model can be defined as follows,

$$\begin{aligned} v_k \,|\alpha \;&\sim Beta\,(1,\alpha)\,, \\ \theta_k \,|G_0 \;&\sim G, \\ z_j \,|\theta\,(\pi) \;&\sim \text{Multi}\,(\theta\,(\pi))\,,\; x_j \,|z_j = k \\ \theta_k \;&\sim p\,(Y\,|\theta_k)\,, \\ \lambda_k \,\left|\left\{x_i, y_i, z_j = k\right\}\right. \;&\sim p\,(\lambda_k \,|X, Y)\,. \end{aligned} \tag{10}$$

where λ_k is the hyperparameter of GPR in cluster k.

The proposed DP-GPR super-resolution model uses a unify framework to combine the DP and GPR. The hyperparameters of the model can be estimated through utilizing MCMC algorithm [33]. The Markov chain is obtained by Gibbs sampling approach, in which each hyperparamter is updated in turn by sampling from the posterior distributions on all other hyperparamters.

With the assumption that GPR tasks are independent identically distributed (i.i.d) for each cluster, the likelihood function of the training dataset is written as

$$p\,(Y|X,\lambda) = \prod_k p\,(Y|X,\lambda_k) p\left(z_j = k|X, Y, (\alpha,\pi)\right). \tag{11}$$

It can be rewritten as

$$\begin{aligned} \log p\,(Y\,|X,\lambda) = \sum_k \left(\prod_j p\,([y_i : z_i = k]\,|[x_i : z_i = k]\,,\lambda_k)\right) \\ \cdot p\left(z_j = k\,|X, Y, (\alpha,\pi)\right). \end{aligned} \tag{12}$$

In the model, the DPMM concentration parameter α, GP parameters λ and indicator variables z are updated by inference on the posterior distribution. In the following, Gibbs sampling is adopted to represent the posterior of the Gibbs sampling.

From Ref. [33], [34], the concentration parameter α can be updated using the Metropolis-Hasting algorithm. The posterior can be written as

$$p\,(\alpha\,|K,N) \propto p\,(\alpha)\,p\,(K\,|\alpha,N)\,. \tag{13}$$

$$p\,(\alpha\,|K,N) \propto p\,(\alpha)\,\frac{\alpha^K \Gamma\,(\alpha)}{\Gamma\,(N+\alpha)}. \tag{14}$$

Similar to equation (8), the posterior distributions of the hyperparameters are proportional to the marginal likelihood. The joint distributions of the hyperparameters can be estimated as follows,

$$\begin{aligned} &p\,(\lambda, Z, \pi, V\,|X, Y) \\ &\quad\propto p\,(Y\,|X\,, Z) \prod_k p\left(z_j = k\,|v_j\right) p\left(v_j\,|\alpha\right) \\ &\quad\cdot \prod_k p\left(\lambda_k\,|X, Y, z_j = k\right). \end{aligned} \tag{15}$$

In order to update the indicator variables z, we also need to inference the posterior conditional distribution of z_i. Let $Z_{-i} = \{z_1, \cdots, z_{i-1}, z_{i+1}, \cdots, z_N\}$,

$$p\,(z_i\,|Z_{-i}, \lambda, X, Y\,) \propto p\,(z_i\,|Z_{-i}, \lambda)\,p\,(X, Y\,|z_i\,, Z_{-i}, \lambda)\,. \tag{16}$$

The detail inference for the optimization can be found in [33], [34], [41], and [42]. Once the parameters of the DP-GPR model are obtained, we can use them to reconstruct the LR image with equation (6).

TABLE 1. An Algorithm for DP-GPR Super-Reconstructing

Input: The HR training dataset Y, LR training dataset X, input test LR image I, size of LR patches and HR patches N, parameters α and β, iteration number max_Iter.

Output: Final SR result $S(I)$,

Training stage

1) Partition LR X_L, Y_H image into N LR patches in raster-scan with one pixel overlapped;
2) Interpolate $X_L = \{x_{L,i}\}_{i=1}^{N}$ into $X = \{x_i\}_{i=1}^{N}$;
3) Draw the center pixel of $Y_H = \{y_{H,i}\}_{i=1}^{N}$ and denote as $Y = \{y_i\}_{i=1}^{N}$;
4) Training the DP-GPR model on $D = \{x_i, y_i\}_{i=1}^{N}$;

Testing stage

5) Interpolate test image I to $S(I)$;
6) Set $T=0$;
7) Partition $S(I)$ image into N HR patches in raster-scan with one pixel overlapped;
8) For each test patch, sample the indictor compute the distance between patches in $S(I)$ with the clusters;
9) For each test patch, update the pixel value with equation (6);
10) Replace the corresponding pixel in $S(I)$;
11) Turn to 7) until $T > max\_Iter$.

Return $S(I)$.

The flowchart of the proposed method is shown in Fig.1 and the detail steps of the proposed method are given in Table 1 .

The computational complexity of the proposed method is mainly determined by two parts, i.e., Gibbs sampling for updating the indicators and Hybrid Monte Carlo for optimizing the hyperparameters of GP covariance function. Assume there are totally M components, since each of Gibbs sample take about $O\left(n^2/M^2\right)$ computations, the process of modeling the distribution for an iteration requires $O\left(n^3/M\right)$.

IV. EXPERIMENTAL RESULTS AND ANALYSIS

To illustrate the validity of our proposed algorithm for single image super-resolution reconstruction, we conduct $3\times$ magnification experiments on the same test images as in [35] and [36], which is commonplace in single image super-resolution. The dataset contains various test images containing persons, plants, animals and buildings. We compare the proposed method with five state-of-the-art approaches including the NE [16], Sparse Coding (SCSR) [19], Gaussian process regression (GPRSR) [22], Active-Sampling Gaussian Process Regression method (AGPSR) [24] and Convolutional neural networks (SRCNN) [37]. The performance of different algorithms is evaluated by three objective quality assessment methods, i.e., peak signal to noise ratio (PSNR), structural similarity (SSIM) and feature similarity (FSIM) [38]–[40].

A. EXPERIMENTAL CONFIGURATION

In our experiments, we use the same 69 HR training images as [19] to prepare our training database, and these training images do not include any image in the testing set. To imitate the real imaging system, all the training images are first blurred by a 5×5 Gaussian filter with standard deviation 1.6, and down sampled by using the bicubic interpolation with scaling factor of 3 to obtain the corresponding LR images. The test images are also degraded by this model.

TABLE 2. Parameter Configurations

Methods	Parameters
NE	k=15
SCSR	dictionary-size=1024, patch-size=5, overlap=4, λ=0.15
AGPRSR	scale-parameter=0.2, active-sampling-ratio=0.01, λ=0.2
DP-GPR	patch-size=5, overlap=4, iteration-number=16, α=0.1 , β=0.01

Because human eyes are more sensitive to luminance changes, we implement all the SR methods on the luminance component and directly enlarge the chromatic components to the desired size with the bicubic interpolation. For SRCNN and GPRSR methods, we keep the default parameters. In the DP-GPR model, the parameter K is the number of clusters generated by DP model, and the number of clusters is determined adaptively according to different training dataset. The parameters of the other methods are listed in Table 2.

B. EXPERIMENTAL RESULTS

Table 3 presents the quantitative results on the 9 test images by different methods, each image has three rows, the first row is PSNR value, the second row is SSIM value, and the last row is FSIM value. These values show clearly that the proposed method produce more competitive results than the other methods. The average PSNR, SSIM and FSIM gains of the proposed method over the second best method (i.e., the AGPSR method) are 0.37 dB, 0.01, and 0.003, respectively.

To further demonstrate the visual quality of the SR results produced by different methods, the $3\times$magnification results of images "Butterfly", "Parrot" and "Flower" using various algorithms are compared in Fig.2∼Fig.4 respectively. It can be seen that the Bicubic interpolation method produces blurred and jaggy artifacts along the edge regions. NE method can reduce the jaggy effects, but it introduces the more blurred edges. The SCSR method can recover high-frequency details while simultaneously it produces over smooth results with unnatural details. GPSR method produces comparable results with sharpen edges. However, it also produces noticeable artifacts along the edge regions, particularly in the reconstruction of image "Butterfly" and image "Parrot". Although SRCNN method produces comparable quantitative results, there remain noticeable blurred artifacts in the zoomed local regions. The AGPGR method achieved pleasing results, but

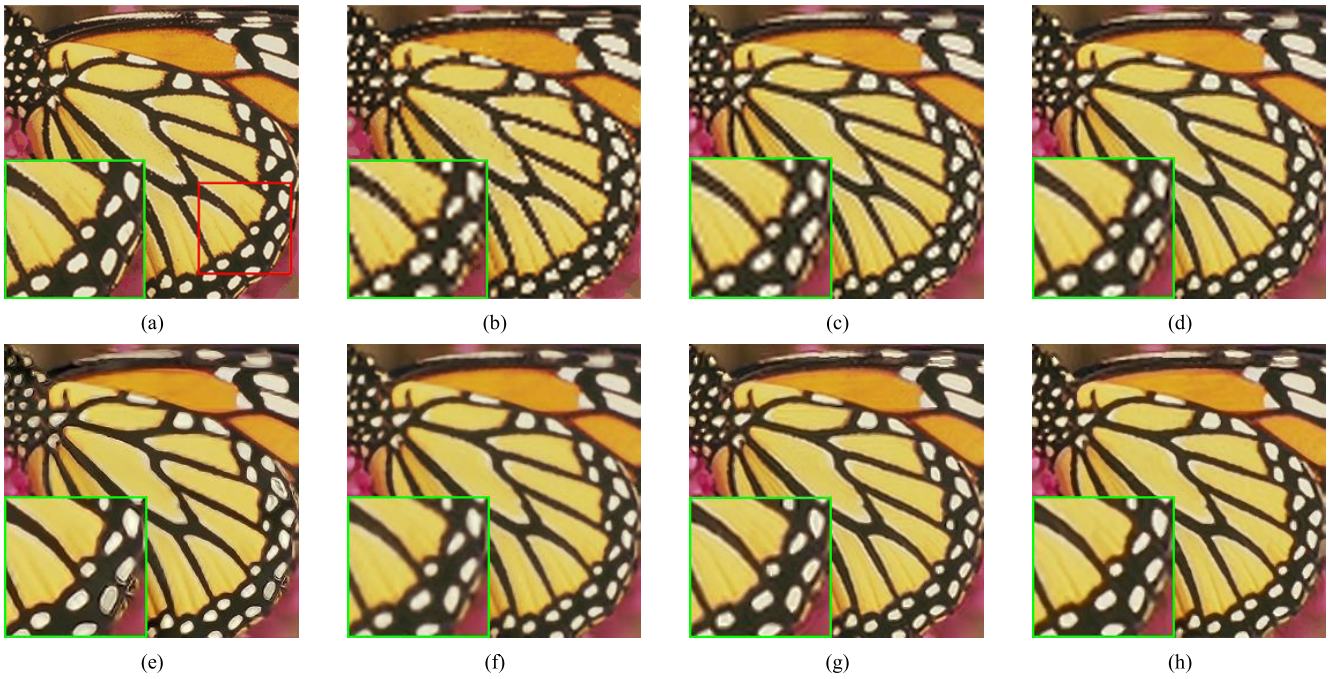

FIGURE 2. Comparison results on "Butterfly" image by different methods (s=3). (a) the original image, (b) Bicubic method, (c) NE method, (d) SCSR method, (e) GPRSR method, (f) SRCNN method, (f) AGPRSR method, (h) the DP-GPR method.

TABLE 3. PSNR (dB), SSIM and FSIM Results by Different Reconstruction Methods (s=3)

Images	Butterfly	Parrot	Parthenon	Bike	Flower	Girl	Hat	Plants	Raccoon	Average
Bicubic	23.51	27.44	24.42	22.02	26.65	31.53	28.21	30.50	27.30	26.84
	0.823	0.880	0.687	0.712	0.792	0.778	0.825	0.872	0.721	0.788
	0.817	0.926	0.815	0.829	0.866	0.904	0.874	0.904	0.875	0.868
NE [16]	25.23	28.07	26.08	23.25	27.63	32.63	29.94	31.47	28.29	28.06
	0.869	0.884	0.697	0.727	0.796	0.800	0.850	0.879	0.719	0.802
	0.852	0.923	0.791	0.814	0.858	0.889	0.872	0.904	0.834	0.860
GPRSR [22]	25.00	28.78	26.35	23.42	28.16	33.23	29.79	31.88	28.95	28.40
	0.835	0.893	0.717	0.744	0.819	0.823	0.849	0.888	0.766	0.815
	0.795	0.915	0.811	0.826	0.869	0.912	0.872	0.901	0.876	0.864
SCSR [19]	25.47	28.92	26.46	23.62	28.28	33.22	30.11	32.15	28.94	28.57
	0.859	0.897	0.723	0.757	0.825	0.822	0.858	0.894	0.765	0.822
	0.826	0.934	0.818	0.834	0.879	0.914	0.886	0.913	0.876	0.875
SRCNN [37]	26.69	29.81	26.92	24.17	28.81	33.37	30.51	32.89	29.09	29.14
	0.892	0.907	0.733	0.771	0.833	0.818	0.856	0.903	0.750	0.829
	0.888	0.938	0.818	0.842	0.886	0.905	0.890	0.923	0.856	0.883
AGPSR [24]	26.73	30.24	26.49	24.04	28.74	33.28	30.63	33.23	28.92	29.15
	0.897	0.910	0.731	0.779	0.834	0.820	0.861	0.907	0.759	0.833
	0.892	0.943	0.825	0.857	0.887	0.917	0.905	0.931	0.875	0.892
DP-GPR	**27.92**	**29.80**	**26.79**	**24.61**	**28.97**	**33.38**	**31.36**	**33.59**	**29.09**	**29.50**
	0.918	**0.907**	**0.738**	**0.799**	**0.844**	**0.824**	**0.879**	**0.911**	**0.764**	**0.843**
	0.917	**0.940**	**0.828**	**0.857**	**0.890**	**0.915**	**0.903**	**0.931**	**0.873**	**0.895**

the recovered details are incomparable to these by the proposed method. The proposed method can afford clearer image edges and richer texture detail without noticeable artifacts.

C. ANALYSIS OF PATCH SIZE

The size of image patch plays an important role in the proposed method. Too large patch size will lead to blurred edges and losing of detailed texture; too small patch size will lead to unwanted artifacts and jaggy effects. In order to evaluate the influence of the patch size on SR results, we perform a set of experiments on the test images with different patch sizes including 3×3, 5×5, 7×7, 9×9 and 11×11.

We first trained the GPR models with different patch sizes, and then we applied these GPR models to the 9 test images.

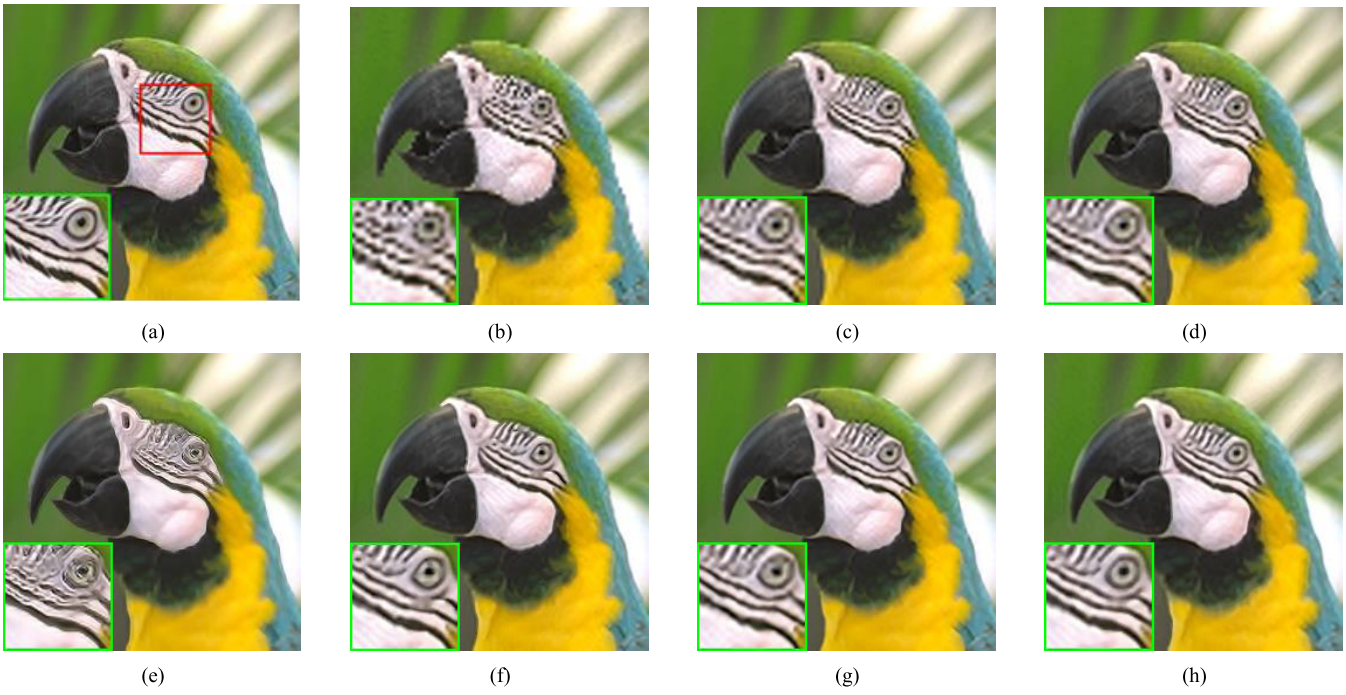

FIGURE 3. Comparison results on "Parrot" image by different methods (s=3). (a) the original image, (b) Bicubic method, (c) NE method, (d) SCSR method, (e) GPRSR method, (f) SRCNN method, (g) AGPRSR method, (h) the DP-GPR method.

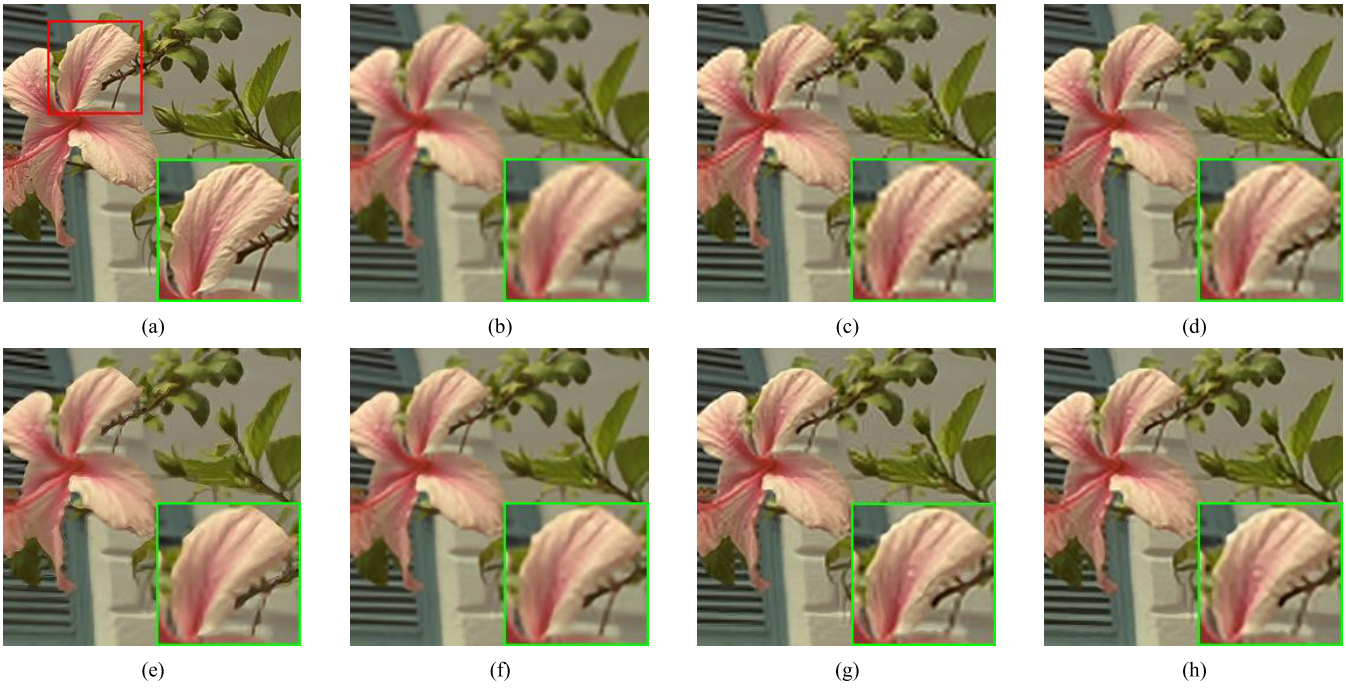

FIGURE 4. Comparison results on "Flower" image by different methods (s=3). (a) the original image, (b) Bicubic method, (c) NE method, (d) SCSR method, (e) GPRSR method, (f) SRCNN method, (g) AGPRSR method, (h) the DP-GPR method.

The experimental results with different patch sizes are presented in Table 4, from which we can see that different patch sizes lead to different PSNR, SSIM, and FSIM values. It is clear that the best results are obtained when the patch size is defined as 5×5. Fig.5-7 present the SR results of the "Butterfly" image and "Flower" image and "Hat" image from different patch sizes, from which we can see that a smaller patch size (e.g., 3×3) produces some unwanted

FIGURE 5. Comparison of SR results on "Butterfly" image with different patch sizes (s=3). (a) Original. (b) 3×3 result. (c) 5×5 result. (d) 7×7 result. (e) 9×9 result. (f) 11×11 result.

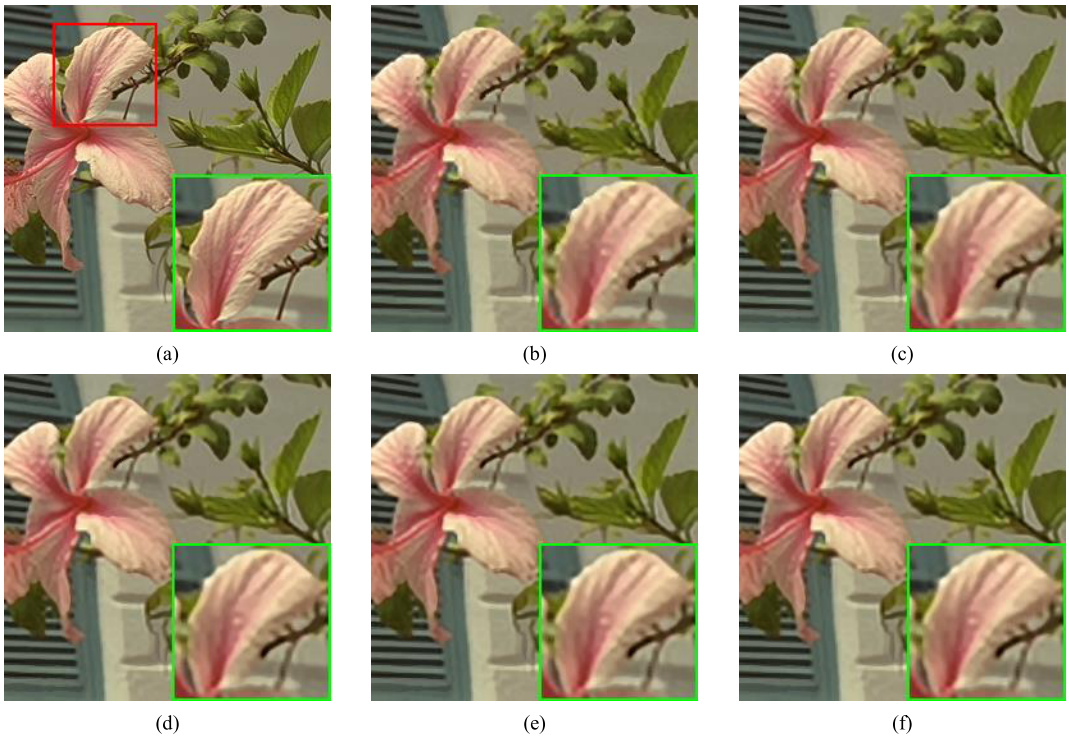

FIGURE 6. Comparison of SR results on "Flower" image with different patch sizes (s=3). (a) Original. (b) 3×3 result. (c) 5×5 result. (d) 7×7 result. (e) 9×9 result. (f) 11×11 result.

artifacts and a larger patch size (e.g., 11×11) produces blurring results. Therefore, we adopt 5×5 as the image patch size in our implementation.

D. ANALYSIS OF THE NUMBER OF ITERATIONS

The number of iterations in testing process has a great influence on the performance of iteration-based SR approach.

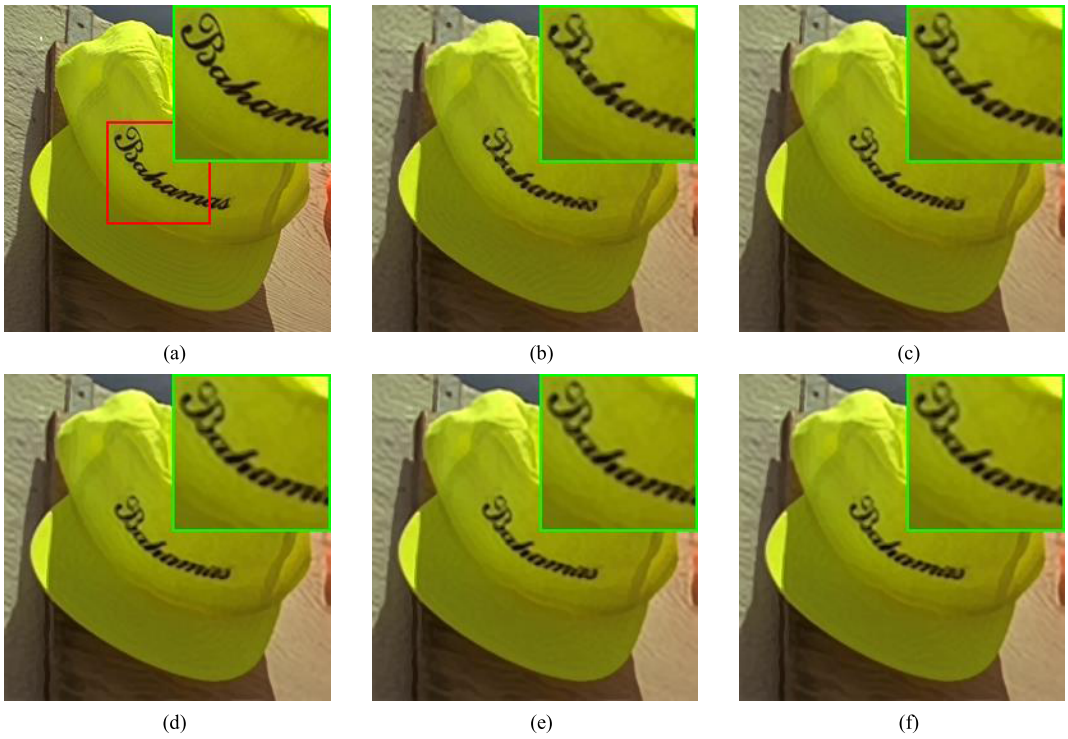

FIGURE 7. Comparison of SR results on "Hat" image with different patch sizes (s=3). (a) Original. (b) 3×3 result. (c) 5×5 result. (d) 7×7 result. (e) 9×9 result. (f) 11×11 result.

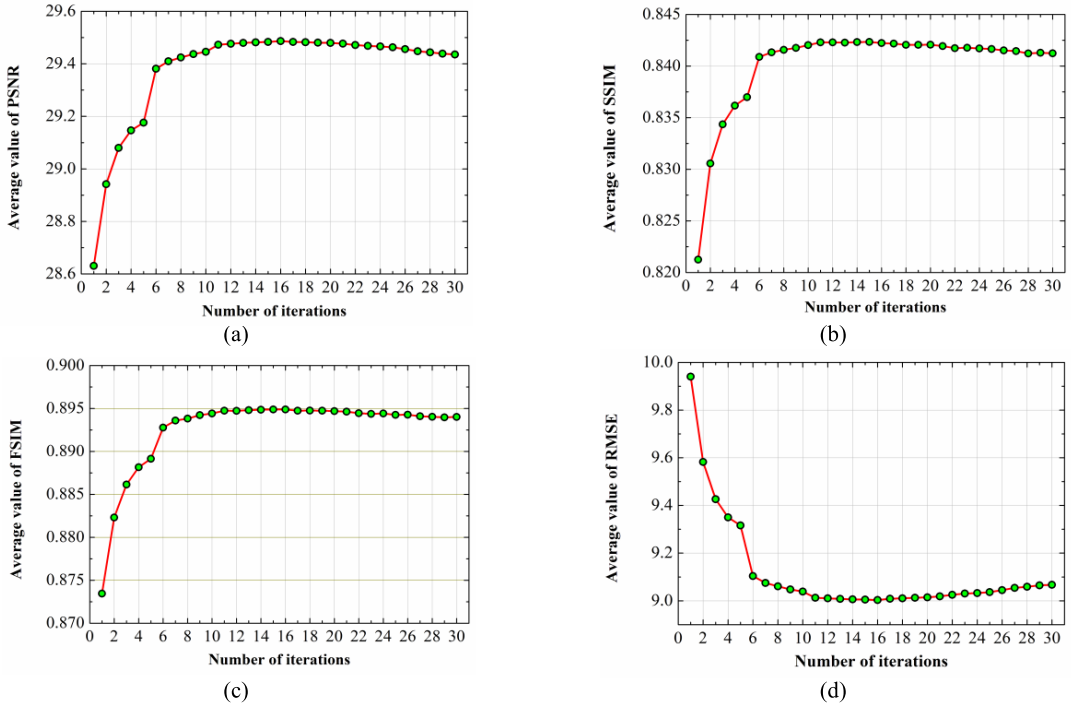

FIGURE 8. Average curves with different iterations. (a) PSNR. (b) SSIM. (c) FSIM. (d). RMSE.

Less iteration will lead to poor reconstruction quality, and too much iteration will increase the running time. Thus, it is necessary for us to conduct a set of experiments to determine the right number of iterations. We perform the experiments oneach test image by changing the number of iterations from 1 to 30. The curved lines of the average values

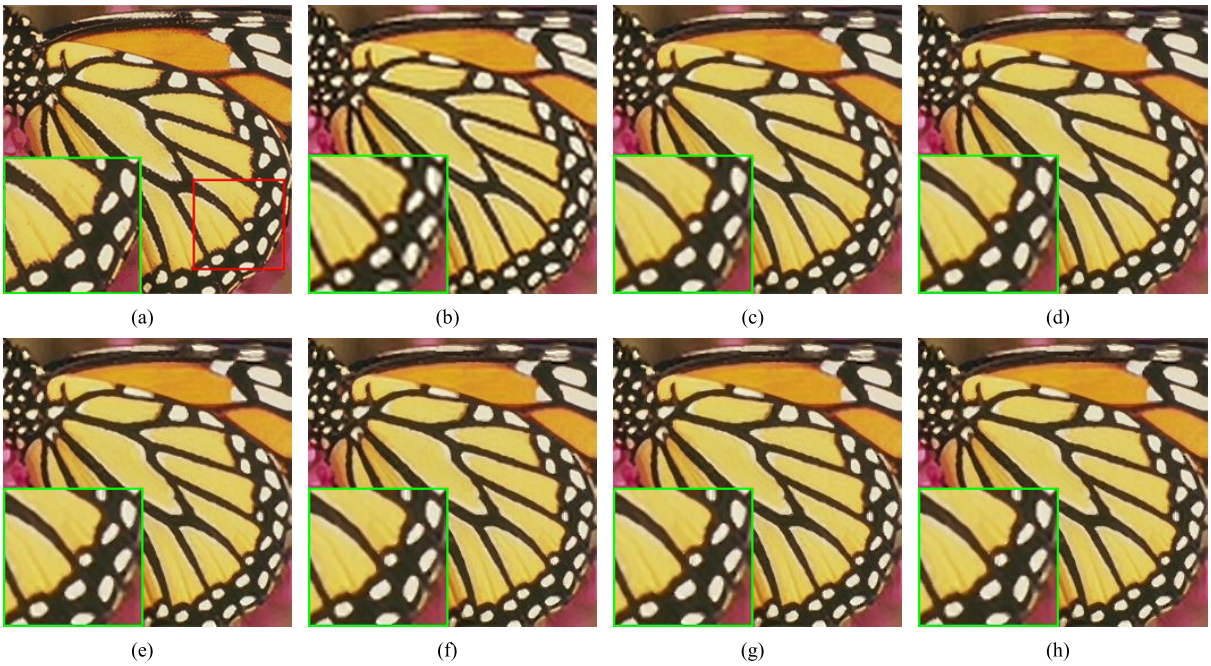

FIGURE 9. Comparison of SR results on "Butterfly" image with different iterations number. (a) Original. (b) 1. (c) 6. (d) 11. (e) 16. (f) 21. (g) 26. (h) 30.

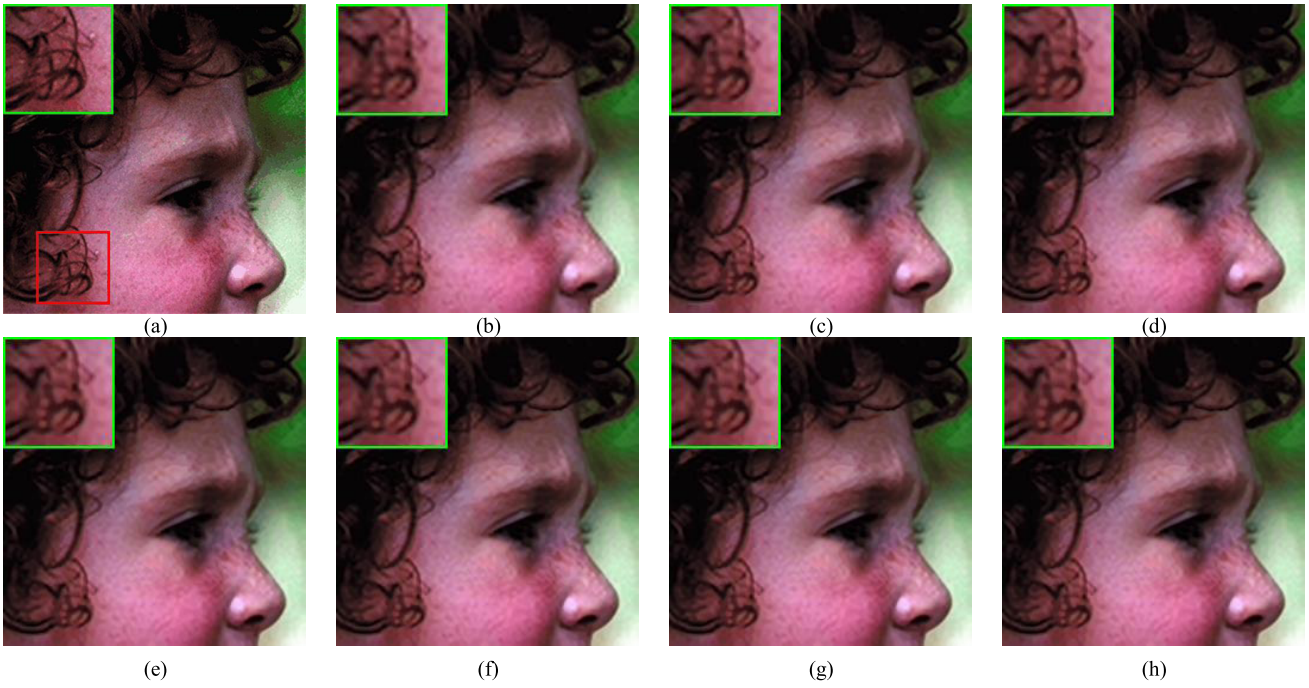

FIGURE 10. Comparison of SR results on "Girl" image with different iterations number. (a) Original. (b) 1. (c) 6. (d) 11. (e) 16. (f) 21. (g) 26. (h) 30.

of PSNR, SSIM, FSIM and RMSE varying with the number of iterations for the 9 test images are plotted in Figs.8.

As shown in Fig.8(a), the value of PSNR increase rapidly with the increasing number of iterations, when the number of iterations reaches 6, the values of PSNR begin to rise slowly, peak value of PSNR can be achieved when the number of iterations is 16, and then it begins to decrease moderately. The same tendency of SSIM and FSIM are presented in Fig.8(b) and Fig.8(c) while the inverse tendency of RMSE is presented in Fig.8(d). We can conclude from the above experiments that good performance can be achieved when the number of iterations is set to be 16.

TABLE 4. PSNR (dB), SSIM and FSIM Results by Different Patch Size (s=3)

Images	Butterfly	Parrot	Parthenon	Bike	Flower	Girl	Hat	Plants	Raccoon	Average
3×3	26.90	29.09	26.31	23.88	28.48	33.13	30.74	32.90	28.78	28.91
	0.908	0.901	0.728	0.782	0.838	0.820	0.874	0.906	0.756	0.835
	0.906	0.933	0.826	0.851	0.887	0.913	0.905	0.929	0.871	0.891
5×5	27.92	29.80	26.79	24.61	28.97	33.38	31.36	33.59	29.09	29.50
	0.918	0.907	0.738	0.799	0.844	0.824	0.879	0.911	0.764	0.843
	0.917	0.940	0.828	0.857	0.890	0.915	0.903	0.931	0.873	0.895
7×7	27.81	29.94	26.75	24.50	28.92	33.34	31.17	33.39	29.05	29.43
	0.915	0.904	0.735	0.792	0.842	0.822	0.875	0.908	0.761	0.839
	0.911	0.938	0.826	0.851	0.888	0.914	0.898	0.928	0.871	0.892
9×9	27.63	29.97	26.69	24.47	28.81	33.30	31.07	33.29	29.03	29.36
	0.913	0.904	0.733	0.789	0.840	0.820	0.874	0.907	0.758	0.838
	0.906	0.938	0.825	0.851	0.886	0.913	0.898	0.927	0.870	0.890
11×11	27.54	29.97	26.68	24.44	28.79	33.30	31.02	33.21	29.06	29.33
	0.910	0.904	0.732	0.788	0.839	0.820	0.873	0.907	0.759	0.834
	0.900	0.939	0.824	0.849	0.886	0.914	0.896	0.926	0.871	0.890

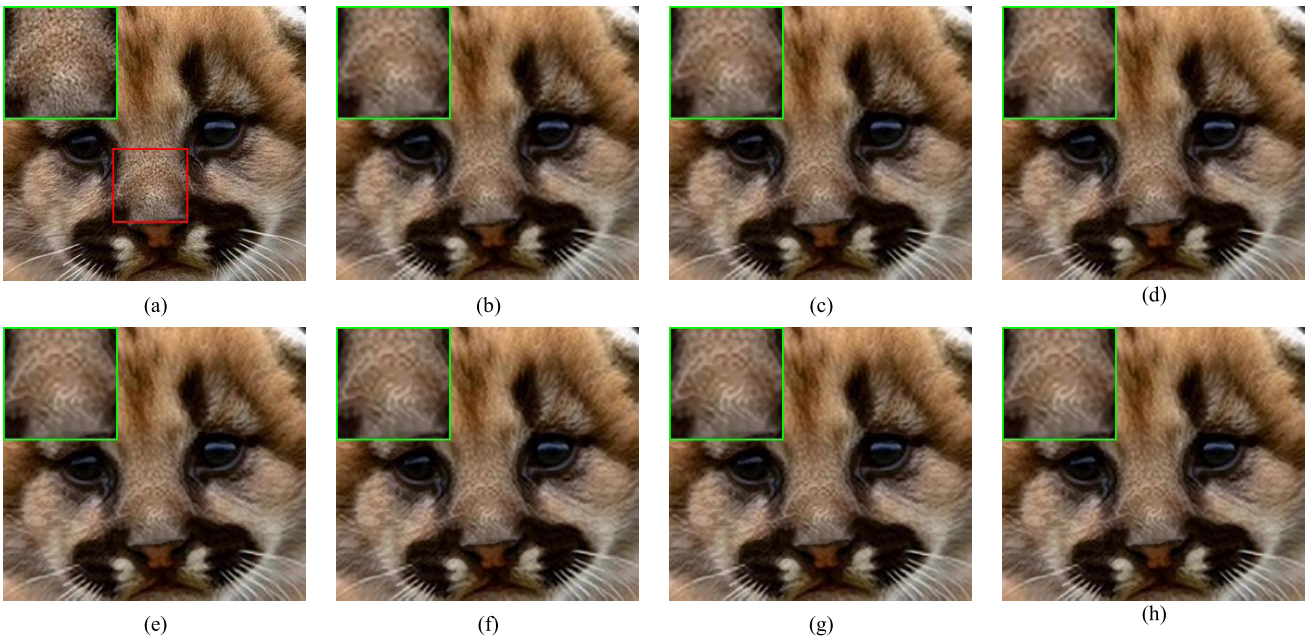

FIGURE 11. Comparison of SR results on "Raccoon" image with different iterations number. (a) Original. (b) 1. (c) 6. (d) 11. (e) 16. (f) 21. (g) 26. (h) 30.

Fig. 9-11 visually demonstrates the reconstructed results obtained by our method on "Butterfly" image, "Girl" image and "Raccoon" image using different number of iterations. We can observe that fewer iterations (i.e., n=1) produce blurred and jagged edges in the SR result, when the number of iterations is larger than 16, the SR images are strongly resembling to each other. Thus, the optimal number of iterations is set to 16.

V. CONCLUSIONS

This paper proposes an effective super-resolution approach based on Dirichlet process and Gaussian process regression. The method can discover the number of clusters automatically and at the same time, the method can obtain more accurate regression model on one cluster. The parameters and hyperparameters have been inferred simply and effectively via Gibbs sampling. The proposed method can adaptively

deal with large-scale and complex distributed data. The objective and subjective assessments on the benchmark test images suggest the effectiveness of the proposed SR method.

Although the proposed method is effective in SR reconstruction, there is still room to boost up the performance of the method. The optimization and computational complexity of nonparametric Bayesian model is still an opening problem, and the reconstruction result would be influenced. On the other hand, the super-resolution for LR image is pixel by pixel. Hence the prediction does not involve semantic information for edge or texture. It is a worthy investigation to develop the method to handle more complex feature in the real application.

REFERENCES

[1] S. C. Park, M. K. Park, and M. G. Kang, "Super-resolution image reconstruction: A technical overview," *IEEE Signal Process. Mag.*, vol. 20, no. 3, pp. 21–36, May 2003.

[2] J. D. van Ouwerkerk, "Image super-resolution survey," *Image Vis. Comput.*, vol. 24, no. 10, pp. 1039–1052, 2006.

[3] J. Tian and K.-K. Ma, "A survey on super-resolution imaging," *Signal, Image Video Process.*, vol. 5, no. 3, pp. 329–342, 2011.

[4] L. Yue, H. Shen, J. Li, Q. Yuan, H. Zhang, and L. Zhang, "Image super-resolution: The techniques, applications, and future," *Signal Process.*, vol. 128, pp. 389–408, Nov. 2016.

[5] W. T. Freeman, T. R. Jones, and E. C. Pasztor, "Example-based super-resolution," *IEEE Comput. Graph. Appl.*, vol. 22, no. 2, pp. 56–65, Mar./Apr. 2002.

[6] W. Hu, G. Cheung, X. Li, and O. C. Au, "Graph-based joint denoising and super-resolution of generalized piecewise smooth images," in *Proc. IEEE Int. Conf. Image Process.*, Sep. 2015, pp. 2056–2060.

[7] H. Takeda, S. Farsiu, and P. Milanfar, "Kernel regression for image processing and reconstruction," *IEEE Trans. Image Process.*, vol. 16, no. 2, pp. 349–366, Feb. 2007.

[8] S. Farsiu, M. D. Robinson, M. Elad, and P. Milanfar, "Fast and robust multiframe super resolution," *IEEE Trans. Image Process.*, vol. 13, no. 10, pp. 1327–1344, Oct. 2004.

[9] H. Hu and L. P. Kondi, "A regularization framework for joint blur estimation and super-resolution of video sequences," in *Proc. IEEE Int. Conf. Image Process.*, Sep. 2005, pp. 329–332.

[10] X. Li, Y. Hu, X. Gao, D. Tao, and B. Ning, "A multi-frame image super-resolution method," *Signal Process.*, vol. 90, no. 2, pp. 405–414, Feb. 2010.

[11] S. P. Belekos, N. P. Galatsanos, and A. K. Katsaggelos, "Maximum *a posteriori* video super-resolution with a new multichannel image prior," *IEEE Trans. Image Process.*, vol. 19, no. 6, pp. 1451–1464, Jun. 2010.

[12] K. I. Kim and Y. Kwon, "Example-based learning for single-image super-resolution," in *Proc. 30th DAGM Symp. Pattern Recognit.*, Sep. 2008, pp. 456–465.

[13] K. I. Kim and Y. Kwon, "Single-image super-resolution using sparse regression and natural image prior," *IEEE Trans. Pattern Anal. Mach. Intell.*, vol. 32, no. 6, pp. 1127–1133, Jun. 2010.

[14] D. H. Trinh, M. Luong, F. Dibos, J.-M. Rocchisani, C.-D. Pham, and T. Q. Nguyen, "Novel example-based method for super-resolution and denoising of medical images," *IEEE Trans. Image Process.*, vol. 23, no. 4, pp. 1882–1895, Apr. 2014.

[15] C. Deng, J. Xu, K. Zhang, D. Tao, X. Gao, and X. Lim, "Similarity constraints-based structured output regression machine: An approach to image super-resolution," *IEEE Trans. Neural Netw. Learn. Syst.*, vol. 27, no. 12, pp. 2472–2485, Dec. 2016, doi: 10.1109/TNNLS.2015.2468069.

[16] H. Chang, D. Y. Yeung, and Y. Xiong, "Super-resolution through neighbor embedding," in *Proc. IEEE Conf. Comput. Vis. Pattern Recognit. (CVPR)*, Sep. 2004, pp. 275–282.

[17] T.-M. Chan, J. Zhang, J. Pu, and H. Huang, "Neighbor embedding based super-resolution algorithm through edge detection and feature selection," *Pattern Recognit. Lett.*, vol. 30, no. 5, pp. 494–502, Apr. 2009.

[18] R. Timofte, V. De, and L. Van Gool, "Anchored neighborhood regression for fast example-based super-resolution," in *Proc. IEEE Int. Conf. Comput. Vis. (ICCV)*, Oct. 2013, pp. 1920–1927.

[19] J. Yang, J. Wright, T. S. Huang, and Y. Ma, "Image super-resolution via sparse representation," *IEEE Trans. Image Process.*, vol. 19, no. 11, pp. 2861–2873, Nov. 2010.

[20] T. Peleg and M. Elad, "A statistical prediction model based on sparse representations for single image super-resolution," *IEEE Trans. Image Process.*, vol. 23, no. 6, pp. 2569–82, Jun. 2014.

[21] M. E. Tipping and C. M. Bishop, "Bayesian image super-resolution," *Adv. Neural Inf. Process. Syst.*, vol. 15, pp. 1279–1286, Mar. 2003.

[22] H. He and W.-C. Siu, "Single image super-resolution using Gaussian process regression," in *Proc. IEEE Conf. Comput. Vis. Pattern Recognit. (CVPR)*, Sep. 2011, pp. 449–456.

[23] Y. Kwon *et al.*, "Efficient learning of image super-resolution and compression artifact removal with semi-local Gaussian processes," *IEEE Trans. Pattern Anal. Mach. Intell.*, vol. 37, no. 9, pp. 1792–1805, Sep. 2015.

[24] H. Wang, X. Gao, K. Zhang, and J. Li, "Single-image super-resolution using active-sampling Gaussian process regression," *IEEE Trans. Image Process.*, vol. 25, no. 2, pp. 935–948, Feb. 2016.

[25] F. M. Schleif, "Generic probabilistic prototype based classification of vectorial and proximity data," *Neurocomputing*, vol. 154, pp. 208–216, Apr. 2015.

[26] M. Zhou *et al.*, "Nonparametric Bayesian dictionary learning for analysis of noisy and incomplete images," *IEEE Trans. Image Process.*, vol. 21, no. 1, pp. 130–144, Jan. 2012.

[27] N. Akhtar, F. Shafait, and A. Mian, "Bayesian sparse representation for hyperspectral image super resolution," in *Proc. IEEE Conf. Comput. Vis. Pattern Recognit. (CVPR)*, Sep. 2015, pp. 3631–3640.

[28] J. Yang, Z. Wang, Z. Lin, S. Cohen, and T. Huang, "Coupled dictionary training for image super-resolution," *IEEE Trans. Image Process.*, vol. 21, no. 8, pp. 3467–3478, Aug. 2012.

[29] Q. Pan *et al.*, "Semi-coupled dictionary learning with applications to image super-resolution and photo-sketch synthesis," in *Proc. IEEE Conf. Comput. Vis. Pattern Recognit. (CVPR)*, Sep. 2012, pp. 2216–2223.

[30] K. Zhang, X. Gao, D. Tao, and X. Li, "Multi-scale dictionary for single image super-resolution," *Comput. Vis. Pattern Recognit. (CVPR)*, Oct. 2012, pp. 1114–1121.

[31] T. S. Ferguson, "A Bayesian analysis of some nonparametric problems," *Ann. Statist.*, vol. 1, no. 2, pp. 209–230, Mar. 1973.

[32] A. Rodríguez, D. B. Dunson, and A. E. Gelfand, "The nested Dirichlet process," *J. Amer. Statist. Assoc.*, vol. 103, no. 483, pp. 1131–1154, Sep. 2008.

[33] J. Had, "MCMC methods for multi-response generalized linear mixed models: The MCMCglmm R package," *J. Statist. Softw.*, vol. 33, no. 2, pp. 1–22, 2010.

[34] C. E. Rasmussen and Z. Ghahramani, "Infinite mixtures of Gaussian process experts," *Adv. Neural Inf. Process. Syst.*, vol. 14, pp. 881–888, Sep. 2002.

[35] W. Dong, L. Zhang, G. Shi, and X. Li, "Nonlocally centralized sparse representation for image restoration," *IEEE Trans. Image Process.*, vol. 22, no. 4, pp. 1620–1630, Apr. 2013.

[36] P. Cheng, Y. Qiu, K. Zhao, and X. Wang, "A transductive graphical model for single image super-resolution," *Neurocomputing*, vol. 148, pp. 376–387, Jan. 2015.

[37] C. Dong *et al.*, "Learning a deep convolutional network for image super-resolution," *IEEE Trans. Pattern Anal. Mach. Intell.*, vol. 38, no. 2, pp. 295–307, Feb. 2016.

[38] Z. Wang, A. C. Bovik, H. R. Sheikh, and E. P. Simoncelli, "Image quality assessment: From error visibility to structural similarity," *IEEE Trans. Image Process.*, vol. 13, no. 4, pp. 600–612, Apr. 2004.

[39] M. Liu, X. Yang, and Y. Shang, "Image quality assessment based on multiscale geometric analysis," *IEEE Trans. Image Process.*, vol. 18, no. 7, pp. 1409–1423, Jul. 2009.

[40] L. Zhang, L. Zhang, X. Mou, and D. Zhang, "FSIM: A feature similarity index for image quality assessment," *IEEE Trans. Image Process.*, vol. 20, no. 8, pp. 2378–2386, Aug. 2011.

[41] C. E. Antoniak, "Mixtures of Dirichlet processes with applications to Bayesian nonparametric problems," *Ann. Statist.*, vol. 2, no. 6, pp. 1152–1174, Nov. 1974.

[42] S. Sun, "Infinite mixtures of multivariate Gaussian processes," in *Proc. 12th Int. Conf. Mach. Learn. Cybern.*, vol. 12. Oct. 2013, pp. 14–17.

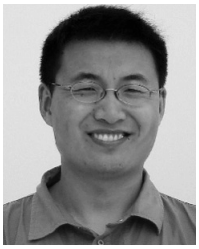

PEITAO CHENG received the B.Sc. and M.Sc. degrees in mechanical manufacturing and automation from Xidian University, Xi'an, China, in 2002 and 2005, respectively, where he is currently pursuing the Ph.D. degree in mechanical manufacturing and automation. Since 2005, he has been with the School of Mechano-Electronic Engineering, Xidian University. His research interests include image processing, machine learning, and artificial intelligence.

YUANYING QIU received the B.Sc. and M.Sc. degrees from Northwestern Polytechnical University, Xi'an, China, in 1981 and 1987, respectively, and the Ph.D. degree from Xidian University, Xi'an, in 2002. From 1999 to 2000, he was with Shizuoka University, Shizuoka, Japan, as a joint-training Ph.D. Student. He is currently the Ph.D. Supervisor and an Academic Leader of Mechanical discipline with the School of Mechano-Electronic Engineering, Xidian University. His research interest covers mechatronics and CAD/CAE/CAM. In these areas, he has authored over 80 papers cited by SCI or EI, respectively. He received the National Science and Technology Progress Award twice, the Shaanxi Provincial Science and Technology Award twice, and the Shaanxi Provincial Teaching Award. He was also nominated as the National 100 Best Ph.D. Dissertations Award.

XIUMEI WANG received the M.Sc. and Ph.D. degrees from Xidian University, Xi'an, China, in 2005 and 2010, respectively. She joined the Department of Electric Engineering, Xidian University, as a Lecturer, in 2010, where he is currently an Associate Professor of Signal and Information Processing. Her research interests are machine learning and image processing. In these areas, she has authored around ten papers.

KE ZHAO received the B.Sc., M.Sc., and Ph.D. degrees in mechanical manufacturing and automation from Xidian University, Xi'an, China, in 1985, 1988, and 1996, respectively. Since 1988, he has been with the School of Mechano-Electronic Engineering, Xidian University. He is currently a Professor of innovation design and intelligent systems. His research interests are product innovation design, computational intelligence, machine learning, and artificial intelligence.